Stretching DNA to twice the normal length with single-molecule hydrodynamic trapping

Yan Jiang[1,2], Theodore Feldman[1,3], Julia A.M. Bakx[4], Darren Yang[1,5], Wesley P. Wong[1,2,5,6*]

[1]Program in Cellular and Molecular Medicine, Boston Children's Hospital, Boston, MA 02115, USA;
[2]Department of Pediatrics, Harvard Medical School, Boston, MA 02115, USA.
[3]VA Boston Healthcare System, Boston, MA 02130, USA.
[4]Department of Physics and Astronomy and LaserLaB, Vrije Universiteit Amsterdam, Amsterdam, The Netherlands.
[5]Wyss Institute for Biologically Inspired Engineering, Harvard University, Boston, MA 02115, USA.
[6]Department of Biological Chemistry and Molecular Pharmacology, Blavatnik Institute, Harvard Medical School, Boston, MA 02115, USA.

* To whom correspondence should be addressed. Tel: 1-617-713-8383; Fax: 1-617-713-8393; Email: wesley.wong@childrens.harvard.edu

Abstract

Single-molecule force spectroscopy has brought many new insights into nanoscale biology, from the functioning of molecular motors, to the mechanical response of soft materials within the cell. Yet in the extreme-force regime, limitations in current approaches have restricted biomolecular studies, particularly under conditions of constant-force and when combined with single-molecule fluorescence. We have met these challenges with a surface-free force spectroscopy approach based on high-speed single-molecule hydrodynamic trapping, which is not only inexpensive and accessible, but also able to probe extremely high tensions. Furthermore, our approach does not require difficult covalent attachment chemistries, and enables simultaneous force application and single-molecule fluorescence. Using this approach, we have induced a recently discovered hyperstretched (HS) state in regions of partially intercalated double-stranded (dsDNA) by applying forces up to 250 pN. The HS state of dsDNA has twice the contour length of B-DNA and was initially discovered under conditions of high tension in the presence of free intercalating dyes. It was hypothesized that regions of HS DNA could also be induced without the aid of intercalators if high-enough forces were applied, but this hypothesis had not been tested until now. Combining force application with single-molecule fluorescence imaging was critical for distinguishing HS DNA from single-stranded DNA that can result from peeling. High-speed hydrodynamic trapping is a powerful yet accessible force spectroscopy method that will be a significant addition to the single-molecule toolbox, enabling the mechanics of nanostructures to be probed in previously difficult to access regimes.

Main text

Single-molecule force spectroscopy has greatly advanced our understanding of macromolecules, illuminating the mechanical properties of nucleic acids, the dynamics of motor proteins, and the kinetics of receptor-ligand binding[1]. Although current approaches for force spectroscopy are powerful and relatively mature, challenges remain—in particular, high force single-molecule measurements, for example in the range above 150 pN, can be difficult to perform. There are a variety of barriers to

making measurements in this regime. Firstly, this force regime is outside the practical range of many standard approaches—for example, optical tweezers can run into problems with available laser power, local heating, or free radical generation, and magnetic tweezers typically do not have strong enough field gradients to generate these forces with standard magnetic microspheres. Secondly, many common surface attachments strategies (e.g biotin-streptavidin or digoxigenin-antidigoxigenin), have limited lifetimes and are rapidly ruptured at these high force[9–12]—as most force spectroscopy methods require samples to be tethered to surfaces[1–8], this limits the amount of force that can be applied on molecules unless more involved covalent conjugation chemistries are used[13]. These problems limit investigations in the high force regime under conditions of constant force or loading rates slow enough to explore near-equilibrium behaviour. In addition, specific and homogeneous surface attachment can often be challenging to carry out, and can potentially lead to artifacts due to denaturation or distortion of molecules at the surface, or the addition of colloidal forces (e.g. Van der Waals) that may be undesirable[14–16].

Here, we present a surface-free force spectroscopy approach that is not only inexpensive and accessible, but also able to probe tensions in the very high force regime without the need for challenging attachment chemistries. This method is based on an active-feedback hydrodynamic trap for particles and cells, pioneered by Schroeder *et al*[17–19] using a cross-slot flow channel[20]. Flow gradients, such as shear and elongational flow [19–24], have been used to induce tension in untethered polymers, but single-molecule observation and force application is usually limited to a low level or a short amount of time as the molecule can simply flow away from the region of interest. Tanyeri *et al*[17,25,26] tackled this problem by combining elongational flow with automated active feedback of the outlet pressure using dual layer PDMS microfluidics. However, the response of their system limited their ability to apply large forces to trapped single-molecules. Using a rigid single-layer device, we have significantly improved the feedback performance of the cross-slot to enable trapping of single molecules under high elongation rates. Our high-speed hydrodynamic trap can trap and apply high forces to single polymers or filaments under elongational flow, enabling us to perform force spectroscopy over a wide range of forces in solution without tethering. We have demonstrated the application of controlled tensions up to 250pN on a single T4 DNA molecule without requiring the attachment of any beads or surfaces. High-speed hydrodynamic trapping can serve as a powerful yet accessible force spectroscopy method, particularly in the high force regime. Furthermore, our approach enables simultaneous monitoring of the sample with single-molecule fluorescence, which can provide essential information about the conformations and functions of biomolecules.

Mechanical studies of DNA have served as a corner stone for single-molecule measurements, and have led to new insights into a range of biological processes[27–36]. DNA has served not only as a subject of study, but also as a tool for the creation of handles and linkages with mechanical signatures, enabling the characterization of variety of molecular structures and functions[37–41]. More generally, the

field of structural DNA nanotechnology has established DNA as a versatile programmable material for the creation of complex nanoscale structures and molecular devices [42,43]. Therefore, a more comprehensive understanding of DNA mechanics would be of great value to both mechanobiology, and to DNA nanotechnology.

dsDNA exhibits complex elastic properties due to its characteristic base stacking and double-helical structure[44]. For example, B-DNA, the structure most commonly found in nature, can transition to different structures under mechanical force. It has been known for over two decades that above a critical overstretching force around 65pN, B-DNA undergoes a transition to reach a contour length of 0.58 nm/bp, 70% over the 0.34 nm/bp of B-DNA [5,45], and it has been established that this can occur in the absence of peeling[46–48]. Recently, a new state of dsDNA with an even longer contour length of 0.7 nm/bp—the maximum length allowed by the standard bond lengths within the backbone of DNA—was discovered under high force in the presence of intercalating dyes[49]. Accordingly, they called this conformation hyperstretched (HS) DNA. Using fluorescently stained single DNA molecules, they were able to confirm that the DNA remained hybridized, and peeling did not occur, and also noted that it was fully intercalated by dyes, with the next-neighbour exclusion rule[50] overcome by force. The authors proposed that HS DNA may be induced on naked DNA without intercalators in the extremely high force regime, yet testing this hypothesis is extremely challenging with standard experimental approaches.

Using our approach, we have stretched regions of partially dye intercalated double-stranded DNA (dsDNA) to twice its normal length by applying forces up to 250 pN. The preserved intercalating dye fluorescence suggests that the two DNA strands remained hybridized. Our result supports the hypothesis that force alone is capable of inducing a recently discovered hyperstretched (HS) state of DNA.

To apply high forces to single DNA molecules, we have developed a high-speed cross-slot hydrodynamic trap that can trap particles under elongational flow using active feedback[17]. In a cross-slot, the fluid flows in from the two inlets (the horizontal channels in Figure 1a) and exits via the two outlets orthogonal to the inlets. This creates a pure elongational field in the cross region. For a filamentous object centered in an elongational flow field, the fluid exerts drag forces against the two halves of the filament in opposite directions, inducing tension in the filament. The center of the cross slot has zero flow velocity and is called a stagnation point. The elongation rate of the flow is defined as the gradient of flow velocity along the direction of flow, which in this case is the rate of velocity increase as the fluid moves away from the stagnation point. Along the inlet axis, particles are always trapped in the center by the converging flow fields in a stable manner, but along the perpendicular outlet direction, small positional deviations from the stagnation point cause the particles to flow away with increasing velocity. Thus, the stagnation point is an unstable saddle point. However, with the

addition of active-feedback, particles can be stability trapped at the stagnation point in both dimensions. As illustrated in Figure 1C, first, the position of the particle is detected by a video camera. Next, depending on the current position of the particle, the stagnation point of the flow field is moved by changing the back pressure in one of the outlets, in order to move the particle in the desired direction. Finally, the particle flows towards the desired trapping position (e.g. center of the field of view) as a result of the shifted flow field. This cycle is rapidly repeated to keep the particle trapped. Published demonstrations of the performance of current dual layer PDMS hydrodynamic traps have shown the effective trapping of particles and cells at elongation rates below 11 s^{-1}. In order to trap single molecules under high elongational flow rates, we improved feedback performance by using a rigid glass microfluidic chip with direct pressure control (Figure 1B and D). One of the outlets is connected to a buffer reservoir filled with pressurized gas, which is controlled by an electronic pressure regulator. The other outlet is connected to a constant pressure source. Buffer injection was also driven by electronically regulated pressurized gas. This allows fast and linear control of the stagnation point position. The microfluidic chip consists of a 40 µm thick double-sided tape with channels cut-out sandwiched between a glass coverglass and a glass slide. The chip was reinforced using UV-cured optical adhesive near the channel region to improve the rigidity. This rigid chip design ensures fast and stable response of the flow to pressure changes. In addition, this chip is very durable, with no degradation in performance over a period of at least a month. Our high-speed trap allows us to trap 500 nm diameter fluorescent particles at an elongation rate over three times the-state-of-art[25]. As shown in Figure 1E and F, the 500 nm fluorescent bead was trapped at elongation rates up to 37.7 s^{-1} with only a moderate increase in positional confinement at these high rates.

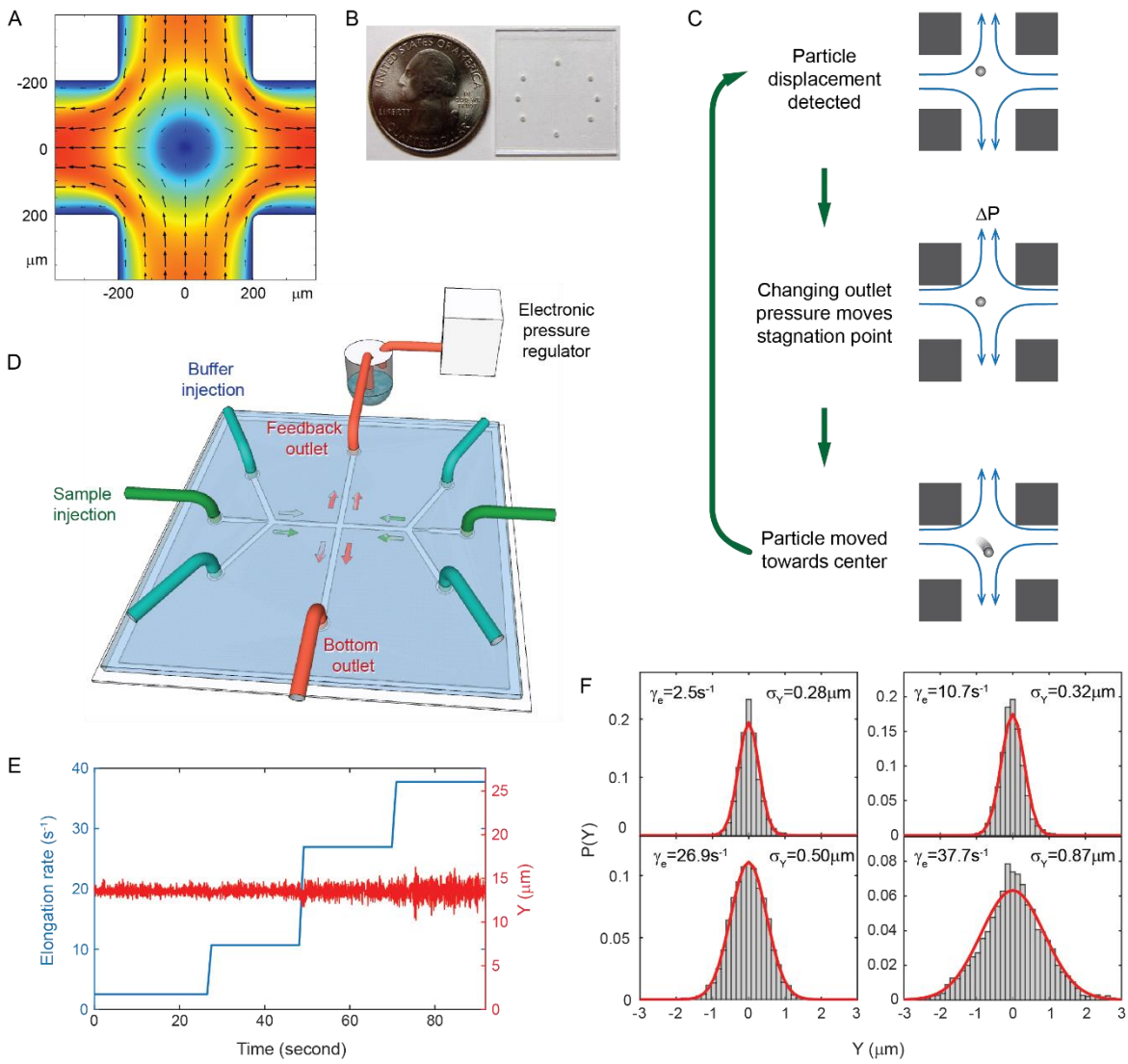

Figure 1 High-speed active-feedback hydrodynamic trap design and performance. A) Elongational flow in cross slot. Small arrows indicate the flow direction. Color indicates the flow velocity with red being the fastest and blue the slowest. B) A photo of an actual hydrodynamic trap chip next to a US quarter coin. C) Schematics of the active feedback mechanism. After the particle displacement was detected, the back pressure in the feedback outlet was adjusted by changing the control voltage of the electronic pressure valve. As a result, the stagnation point moved and the particle was moved by flow towards the center of the cross slot. D) A 3D illustration of the fluidic connections showing the back-pressure control on the upper outlet. E) Y trajectory (red) of a trapped 500 nm fluorescent bead as the elongation rate (blue) stepped up from 2.5 to 37.7 s^{-1}. F) The distribution of the y position at the four different elongation rates.

Using the hydrodynamic trap, we trapped and hyperstretched YOYO-1 labeled T4 DNA in a high viscosity buffer. As shown in Methods, for long filaments, the drag force on each segment is proportional to the flow velocity and therefore the distance from the stagnation point (Figure 2A). As a result, the tension profile along the length of the filament is parabolic. Equation (1) shows the tension in a filament with length L, at a point l distance from the center.

$$T(l) = \int_l^{L/2} f_{drag}(y)dy = \int_l^{L/2} a\mu v(y)dy = \int_l^{L/2} a\mu\gamma_e y dy = \frac{1}{2}a\mu\gamma_e\left(\frac{L^2}{4} - l^2\right) \qquad (1)$$

Here a is a constant depending on the hydrodynamic profile of the filament. Modelling dsDNA as a 2 nm diameter rod, we estimated $a = 0.60$ (Method).

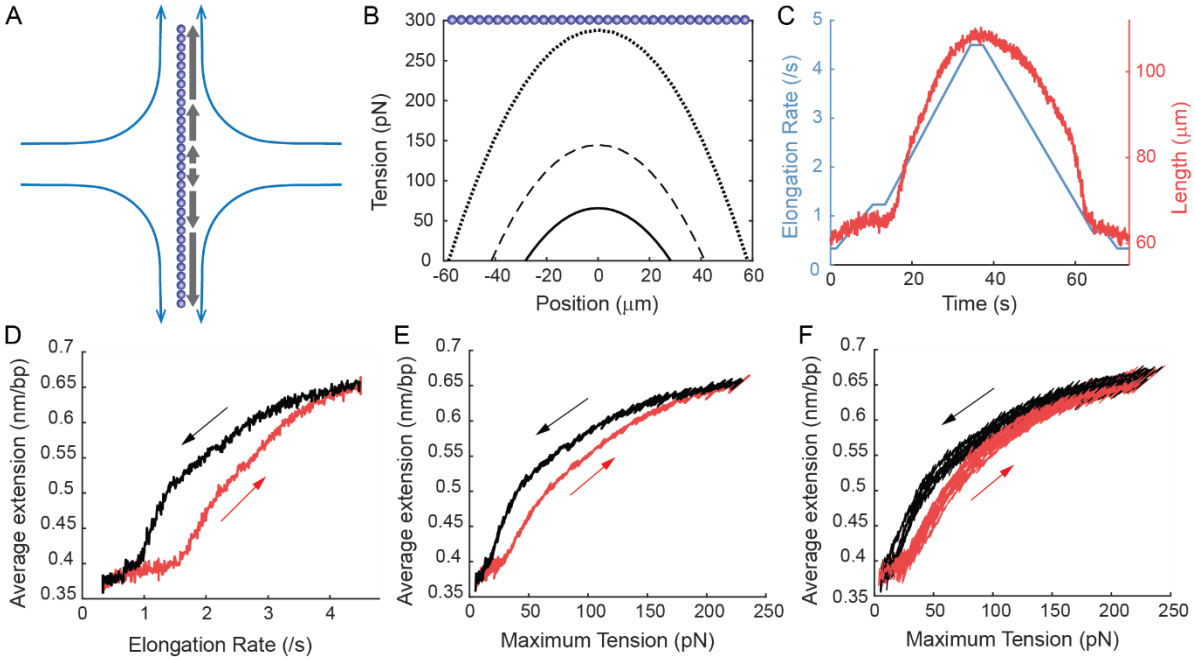

Figure 2 YOYO-1 stained DNA stretching under elongational flow. A) Drag force (block arrows) on each segment of a long filament in elongational flow is proportional to the distance between the segment and the stagnation point. B) Example parabolic tension profile along 56 μm (solid line), 83 μm (dashed line), and 116 μm (dotted line) long dsDNA. A cartoon of a 116 μm polymer is overlaid on the top axis to visualize the tension distribution. C) Time traces of the elongation rate (blue) and DNA end-to-end distance (red). D) DNA end-to-end distance as a function of elongation rate. The red curve is extension and the black curve is relaxation. E) DNA end-to-end distance as a function of the maximum tension in DNA. The red curves are elongation and the black curves are relaxation. F) Overlay of results from 10 experiments. All data shown here was taken with 4:1 labelled DNA.

The maximum tension is at the center of the filament and proportional to the square of the filament length (Figure 2B). The tension is also proportional to the elongation rate and the viscosity. With a combination of a high elongation rate, a high viscosity buffer and long DNA, we were able to induce a maximum of 250 pN tension in DNA. We used bacteriophage T4 GT7 genome DNA with a length of 166 kbps and a contour length of 56.4 μm. We prepared DNA with two different labelling ratios, with nucleic acid base pairs to dye monomer ratios (N:D) of 4:1 and 8:1(Methods). The DNA was stained and trapped in buffer with no salt to prevent the YOYO-1 dye from dissociating. Similar results were observed in buffers with up to 20 mM NaCl. With even higher salt concentrations, the dyes dissociate too fast to allow high-speed trapping. Even though low salt conditions usually shift the equilibrium of stretched dsDNA towards melting[51], the intercalated dyes likely protected the dsDNA from melting[52]. We ramped tension in the trapped DNA up and down by ramping the elongation rate up and down (Figure 2C, Supplementary Movie 1). The maximum tension in the DNA at each time point was calculated using the elongation rate and the measured length of the DNA filament (Figure 2D), and the length of DNA was plotted as a function of the maximum tension (Figure 2E). Because

each intercalated dye monomer increases the contour length of dsDNA by 0.34 nm, the average extension of the intercalated B-form T4 DNA in our experiment was 0.37 nm/bp, when the maximum tension was held at ~ 10pN. The end-to-end distance of T4 DNA increased rapidly when the maximum tension exceeded 25 pN. The slope decreased for tensions above 100 pN. At the maximum elongation rate we applied, the total length of the 4:1 labelled DNA was 0.65 nm/bp, over 90% longer than regular B-DNA, indicating a transition of DNA structure. Because the total end-to-end distance is the sum of many segments, each under different force, the central region of the DNA will be extended longer than the average. From the large average extension, the maximum extension in the central region likely approached the length of the sugar-phosphate backbone, which is twice the contour length of B-DNA. As describe in the next section, we confirmed this by analysing the fluorescence intensity profile. During elongation-relaxation cycles, we observed significant hysteresis that could be reduced by lowering the flow ramping rates. But the hysteresis existed even at the slowest flow ramping rates we could achieve without incurring photodamage during the experiment (Figure 2E and F). Based on the current experiment, we could not distinguish whether this hysteresis was dynamic, meaning that the hyperstretching transition was slow, or static, meaning that the B and HS states were bistable under our experimental conditions. Similar hysteresis was previously reported for dsDNA stretching and relaxation in the presence of intercalating molecules[53–55]. The hysteresis in those cases was attributed to the slow binding/dissociation of the intercalators. However, this cannot explain our observation because there was no free YOYO-1 dye in our experiment.

We also note that it is important to distinguish the hyperstretched state from DNA peeling or bubble formation, which can also dramatically increase the length of DNA by converting regions of dsDNA to single-stranded DNA (ssDNA). As discussed by Schakenraad *et. al.*[49], combining force application with single-molecule fluorescence is key, as DNA peeling can be observed by a sudden reduction in fluorescence intensity in regions of emergent ssDNA. These were not observed under our experimental conditions, as further discussed in the next section. Additionally, within DNA force-extension curves, melting transitions and peeling transitions are typically marked by sharp increases in length during stretching and more significant hysteresis during relaxation—features that were not observed during our experiments[47,48]. Still, we cannot rule out the possibility that small bubbles of melted DNA occurred in the short DNA segments (about 5-13 base pairs) between intercalated dyes. Though, we note again that we did not observe any obvious melting/reannealing signatures in the length vs maximum tension curves for cycles of extension and relaxation.

In addition to measuring the length of the DNA filament as a function of flow-rate, we can also study the force-dependent properties of DNA by analysing the single-molecule fluorescence intensity profile. Because of the unique parabolic tension profile that we impose along each DNA molecule, we can sample a wide range of forces on a single DNA molecule under a single elongation rate. For example, the kymograph in Figure 3A shows the evolution of the intensity profile of a 4:1

labelled DNA molecule at 5 different elongation rates (Figure 3B, Supplementary Movie 2). At low elongation rates, the fluorescence intensity profile is uniform, independent of the tension (Figure 3A and D). At high elongation rates, the intensity remains the same in the lowest tension regions and decreases in the high-tension region (Figure 3E-H). The intensity as a function of tension are consistent across different elongation rates (Figure 3I). The intensity approaches a minimum for forces above 100 pN. Over the course of the experiment, the total intensity of the entire DNA molecule showed slow dissociation of the YOYO-1 dye but no clear changes correlated with changes in the length of the DNA (Figure 3C, Supplementary Figure 2). This suggests that the YOYO-1 did not dissociate, the intensity of each YOYO-1 did not change, and the dsDNA did not peel during the experiment, consistent with a direct transition into the HS state[49,56]. Therefore, the change in intensity profile is mostly due to the change in dye distribution that results from local stretching of the molecule. At low elongation rates, the average extension was 0.42 nm/bp (Figure 3B). As the tension increased, the length of DNA increased and so did the space between bound YOYO-1. Assuming the extension is proportional to the reciprocal of the intensity, we plotted the DNA extension as a function of the tension (Figure 3J). The results from all 5 elongation rates are plotted together to show the overlap between them. The black curve is the average of all the data. At low forces, around 10 pN or lower, the DNA could diffuse in and out of the focal plane, making the measured intensity lower than the actual value. Therefore, this region, to the left of the dashed line in Figure 3I, is not analysed. The extension first slightly increased from 10 to ~25 pN, consistent with the high force region of a worm-like-chain force-extension curve[57]. This suggests that the non-intercalated segments of DNA remained in B-form in this regime. The local extension started to increase above 25 pN, consistent with the end-to-end distance measurements (Figure 2F). This increase in length indicated a gradual transition from B-DNA into HS DNA. The local extension of DNA rapidly increased until ~ 100 pN, and then the increase slowed down for even higher force, suggesting most of the non-intercalated segments of DNA had transitioned to the HS state above 100 pN. As the maximum tension increased, the hyperstretched region expanded (Figure 3A, yellow arrows). Above 200 pN, the local extension of DNA reached ~ 0.7 nm/bp, the contour length of the sugar-phosphate backbone. This curve (Figure 3J) matches well with the DNA hyperstretching curve measured by optical tweezer experiments in the presence of the fast equilibrating dye YO-PRO-1 (Fig. S1 in reference [56]). Both curves feature a slow increase in extension in the low-force regime, a rapid increase until ~100 pN, and a slow increase above 100pN. The lower force regimes of both curves deviate from the usual dsDNA force-extension curves that can be described by the WLC model due to dye intercalation and hyperstretching. This suggests that our estimation of drag force on DNA is reasonably accurate. In their experiment, the gradual transition of DNA from B form to HS form was achieved through the combination of stretching and the intercalation of more dye molecules. In our experiment, as there was no free dye in solution during the stretching experiment, the non-intercalated DNA segments were transitioned to the HS form just by force.

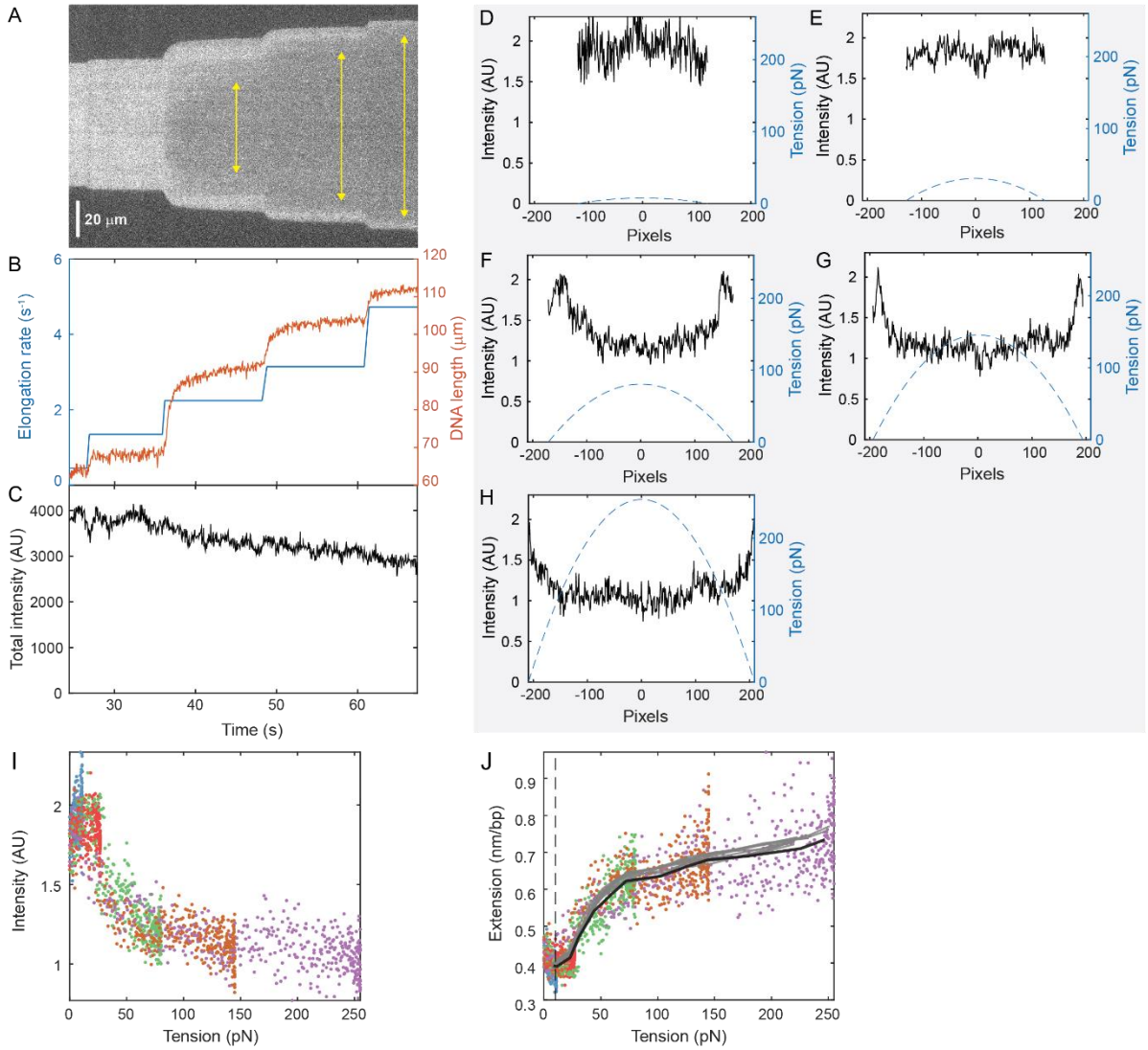

Figure 3 Force-dependent fluorescence intensity profile on 4:1 labelled DNA. A) Kymograph of a T4 DNA in the hydrodynamic trap as the elongation rate was increased in steps. Yellow arrows indicate the hyperstretched region, defined as over 0.6 nm/bp average extension. B) Time traces of the elongation rate and the DNA end-to-end distance. Blue trace is the elongation rate and red trace is the end-to-end distance of DNA. C) Time trace of the total fluorescence intensity on DNA shows no correlation with the DNA length. D-H) The intensity and tension profile of the DNA at 5 different elongation rates. The solid curve is the intensity and the dashed line is the tension. I) The intensity as a function of tension; colored dots are results from 5 different elongation rates. J) The extension per base pair of DNA as a function of tension; colored dots are results from 5 different elongation rates. The black line is the average of these results, and the gray lines are results from 10 other experiments. The region below 10 pN to the left of the dashed line was not analyzed.

The transition to a state with a 0.7 nm/bp contour length was also observed in DNA with a lower staining ratio of 5:1 (Figure 4), providing further evidence that force-alone can induce a transition of DNA into the HS form. At this staining ratio, only approximately 12% of the DNA was intercalated. Because YOYO-1 is a dimer that intercalates into the spaces between four consecutive base pairs[58], this corresponded to an average of 14 base pairs between neighbouring pairs of dimers. Therefore, the majority of the DNA was not intercalated. With this lower staining ratio, the fluorescent signal was weaker, limiting the trapping to lower elongation rates. As a result, the maximum tension we could apply to these DNA molecules in this case was limited to approximately

~ 150 pN. Nevertheless, the entire DNA filament could be stretched to an average distance per base pair ~0.62 nm/bp, longer than the contour length of S-DNA. The force-dependent intensity profile of the 8:1 labelled DNA showed similar behaviour as the 4:1 labelled DNA (Figure 3). The calculated extension as a function of tension from the 8:1 labelled DNA is shown in Figure 4B, demonstrating high similarity to the results for the 4:1 labelled DNA. A direct comparison between these two conditions is presented in Figure 4C, showing an overlay of the results from the two staining ratios, with 10 replicas each. The results are very similar, though we note that the 8:1 labelled DNA molecules have a shorter extensions at low force because of their shorter contour length in the B/I-form[59].

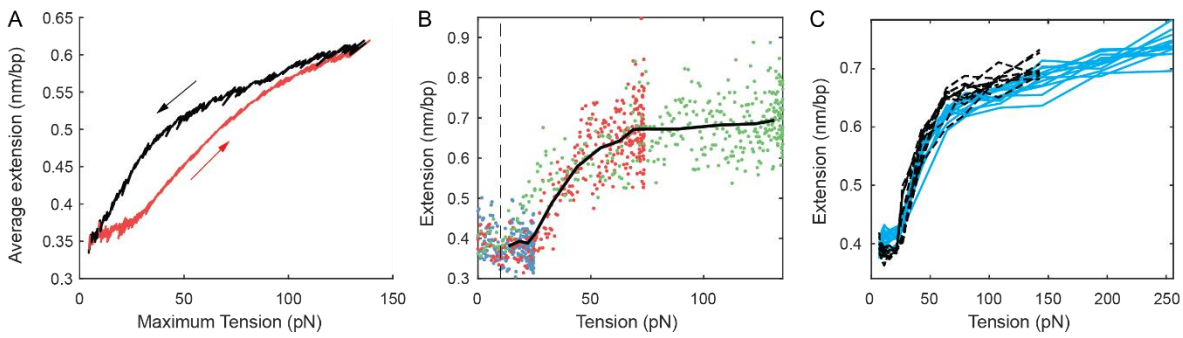

Figure 4 Hyperstretching of 8:1 labelled DNA. A) Time traces of the DNA end-to-end distance as a function of the maximum tension in DNA for 8:1 labelled DNA. The red curves are elongation and the black curves are relaxation. B) The extension per base pair of DNA as a function of tension. The colored dots are results from 3 different elongation rates; the black line is the average of these results. The region below 10 pN to the left of the dashed line was not analyzed. C) Overlay of average force-extension curves from 20 experiments. The 10 red lines are with 4:1 labelled DNA. The 10 black lines are with 8:1 labelled DNA.

Our observation of partially intercalated dsDNA reaching an extension of ~ 0.7 nm/bp under tension in the absence of free intercalators supports the hypothesis that force alone is capable of converting regions of dsDNA from B-form to HS-form. By combining force application with single-molecule fluorescence, we were further able to distinguish this transition from increases in length that can result from DNA peeling, which can also increase the overall sample length by separating dsDNA into strands of ssDNA.

The application of the extremely high forces required by the hyperstretching transition was enabled by our newly developed high-speed hydrodynamic trap. The maximum tension we induced in DNA was ~ 250 pN, perhaps the highest constant stretching force applied to dsDNA in the literature. Our surface-free approach allows simultaneous fluorescence detection and force spectroscopy, especially in force regimes that are traditionally difficult to study. In addition, the system can be less expensive and easier to set up than many commonly used force probes, particularly for users who already have microscopes capable of fluorescence imaging. Additionally, because no bead or surface attachments are needed for this method, sample preparation can also be simplified.

In conclusion, we have demonstrated force-induced hyperstretching of dsDNA to the length of the sugar-phosphate backbone with a high-speed hydrodynamic trap. This experiment not only has implications for understanding the mechanics and structure of DNA under stress, but also demonstrates the potential of the hydrodynamic trap as a powerful yet accessible force spectroscopy method, able to probe molecular mechanics in previously difficult to access regimes.

Conflict of Interest

There are no conflicts to declare.

Acknowledgement

We acknowledge help from the microfluidic prototyping facilities in Wyss Institute for Biologically Inspired Engineering on fabricating the microfluidic chip. We are also grateful to James Pelletier, the MIT Media Lab, and the Microfluidics Core Facility at Harvard Medical for their help in fabricating early versions of the microfluidic chip. This work was supported by National Science Foundation Graduate Research Fellowship DGE-1144152 (D.Y.), NIH NIGMS R35 GM119537 (W.P.W.), and internal support from the Wyss Institute at Harvard (W.P.W.). Funding for the open access charge: National Institutes of Health.

Bibliographic references

(1) Neuman, K. C.; Nagy, A. Single-Molecule Force Spectroscopy: Optical Tweezers, Magnetic Tweezers and Atomic Force Microscopy. *Nat. Methods* **2008**, *5* (6), 491–505. https://doi.org/10.1038/nmeth.1218.

(2) Smith, S.; Finzi, L.; Bustamante, C. Direct Mechanical Measurements of the Elasticity of Single DNA Molecules by Using Magnetic Beads. *Science (80-.).* **1992**, *258* (5085), 1122–1126. https://doi.org/10.1126/SCIENCE.1439819.

(3) Ladoux, B.; Doyle, P. S. Stretching Tethered DNA Chains in Shear Flow. *Europhys. Lett.* **2000**, *52* (5), 511–517. https://doi.org/10.1209/epl/i2000-00467-y.

(4) Kishino, A.; Yanagida, T. Force Measurements by Micromanipulation of a Single Actin Filament by Glass Needles. *Nature* **1988**, *334* (6177), 74–76. https://doi.org/10.1038/334074a0.

(5) Cluzel, P.; Lebrun, A.; Heller, C.; Lavery, R.; Viovy, J. L.; Chatenay, D.; Caron, F. DNA: An Extensible Molecule. *Science* **1996**, *271* (5250), 792–794. https://doi.org/10.1126/science.271.5250.792.

(6) Ashkin, A.; Dziedzic, J. M.; Bjorkholm, J. E.; Chu, S. Observation of a Single-Beam Gradient Force Optical Trap for Dielectric Particles. *Opt. Lett.* **1986**, *11* (5), 288. https://doi.org/10.1364/OL.11.000288.

(7) Strick, T. R.; Allemand, J. F.; Bensimon, D.; Bensimon, A.; Croquette, V. The Elasticity of a Single Supercoiled DNA Molecule. *Science* **1996**, *271* (5257), 1835–1837. https://doi.org/10.1126/science.271.5257.1835.

(8) Hoh, J. H.; Cleveland, J. P.; Prater, C. B.; Revel, J. P.; Hansma, P. K. Quantized Adhesion Detected with the Atomic Force Microscope. *J. Am. Chem. Soc.* **1992**, *114* (12), 4917–4918. https://doi.org/10.1021/ja00038a075.

(9) Merkel, R.; Nassoy, P.; Leung, A.; Ritchie, K.; Evans, E. Energy Landscapes of Receptor-

Ligand Bonds Explored with Dynamic Force Spectroscopy. *Nature* **1999**, *397* (January), 50–53. https://doi.org/10.1038/16219.

(10) Neuert, G.; Albrecht, C.; Pamir, E.; Gaub, H. E. Dynamic Force Spectroscopy of the Digoxigenin-Antibody Complex. *FEBS Lett.* **2006**, *580* (2), 505–509. https://doi.org/10.1016/j.febslet.2005.12.052.

(11) Lipfert, J.; Kerssemakers, J. W. J.; Jager, T.; Dekker, N. H. Magnetic Torque Tweezers: Measuring Torsional Stiffness in DNA and RecA-DNA Filaments. *Nat. Methods* **2010**, *7* (12), 977–980. https://doi.org/10.1038/nmeth.1520.

(12) Friddle, R. W.; Noy, A.; De Yoreo, J. J. Interpreting the Widespread Nonlinear Force Spectra of Intermolecular Bonds. *Proc. Natl. Acad. Sci. U. S. A.* **2012**, *109* (34), 13573–13578. https://doi.org/10.1073/pnas.1202946109.

(13) Janissen, R.; Berghuis, B. A.; Dulin, D.; Wink, M.; van Laar, T.; Dekker, N. H. Invincible DNA Tethers: Covalent DNA Anchoring for Enhanced Temporal and Force Stability in Magnetic Tweezers Experiments. *Nucleic Acids Res.* **2014**, *42* (18), e137. https://doi.org/10.1093/nar/gku677.

(14) Goldstein, L. Kinetic Behavior of Immobilized Enzyme Systems. *Methods Enzymol.* **1976**, *44*, 397–443.

(15) Friedel, M.; Baumketner, A.; Shea, J.-E. Effects of Surface Tethering on Protein Folding Mechanisms. *Proc. Natl. Acad. Sci. U. S. A.* **2006**, *103* (22), 8396–8401. https://doi.org/10.1073/pnas.0601210103.

(16) Shin, Y.; Davis, J. H.; Brau, R. R.; Martin, A.; Kenniston, J. A.; Baker, T. A.; Sauer, R. T.; Lang, M. J. Single-Molecule Denaturation and Degradation of Proteins by the AAA+ ClpXP Protease. *Proc. Natl. Acad. Sci. U. S. A.* **2009**, *106* (46), 19340–19345. https://doi.org/10.1073/pnas.0910484106.

(17) Tanyeri, M.; Johnson-chavarria, E. M.; Schroeder, C. M. Hydrodynamic Trap for Single Particles and Cells. *Appl. Phys. Lett.* **2010**, *96* (22), 224101. https://doi.org/10.1063/1.3431664.

(18) Charles M. Schroeder, †; Eric S. G. Shaqfeh, *,‡ and; Chu§, S. Effect of Hydrodynamic Interactions on DNA Dynamics in Extensional Flow: Simulation and Single Molecule Experiment. **2004**. https://doi.org/10.1021/MA049461L.

(19) Schroeder, C. M.; Babcock, H. P.; Shaqfeh, E. S. G.; Chu, S. Observation of Polymer Conformation Hysteresis in Extensional Flow. *Science* **2003**, *301* (5639), 1515–1519. https://doi.org/10.1126/science.1086070.

(20) Perkins, T. T.; Smith, D. E.; Chu, S. Single Polymer Dynamics in an Elongational Flow. *Science (80-.).* **1997**, *276*, 2016–2021.

(21) De Gennes, P. G.; Gennes, P. G. De. Coil-Stretch Transition of Dilute Flexible Polymers under Ultrahigh Velocity Gradients. *J. Chem. Phys.* **1974**, *60* (12), 5030–5042. https://doi.org/10.1063/1.1681018.

(22) Smith, D. E.; Babcock, H. P.; Chu, S. Single-Polymer Dynamics in Steady Shear Flow. *Science* **1999**, *283* (5408), 1724–1727. https://doi.org/10.1126/SCIENCE.283.5408.1724.

(23) Klotz, A. R.; Soh, B. W.; Doyle, P. S. Motion of Knots in DNA Stretched by Elongational Fields. *Phys. Rev. Lett.* **2018**, *120* (18), 188003. https://doi.org/10.1103/PhysRevLett.120.188003.

(24) Xu, W.; Muller, S. J. Polymer-Monovalent Salt-Induced DNA Compaction Studied via Single-Molecule Microfluidic Trapping. *Lab Chip* **2012**, *12* (3), 647–651. https://doi.org/10.1039/c2lc20880f.

(25) Tanyeri, M.; Schroeder, C. Manipulation and Confinement of Single Particles Using Fluid Flow. *Nano Lett.* **2013**, *13* (6), 2357–2364.

(26) Tanyeri, M.; Ranka, M.; Sittipolkul, N.; Schroeder, C. M. A Microfluidic-Based Hydrodynamic Trap: Design and Implementation. *Lab Chip* **2011**, *11*, 1786–1794. https://doi.org/10.1039/c0lc00709a.

(27) Bustamante, C.; Bryant, Z.; Smith, S. B. Ten Years of Tension: Single-Molecule DNA Mechanics. *Nature* **2003**, *421* (6921), 423–427. https://doi.org/10.1038/nature01405.

(28) Abbondanzieri, E. A.; Greenleaf, W. J.; Shaevitz, J. W.; Landick, R.; Block, S. M. Direct Observation of Base-Pair Stepping by RNA Polymerase. *Nature* **2005**, *438* (7067), 460–465. https://doi.org/10.1038/nature04268.

(29) Wang, M. D.; Schnitzer, M. J.; Yin, H.; Landick, R.; Gelles, J.; Block, S. M. Force and Velocity Measured for Single Molecules of RNA Polymerase. *Science* **1998**, *282* (5390), 902–907. https://doi.org/10.1126/science.282.5390.902.

(30) Smith, D. E.; Tans, S. J.; Smith, S. B.; Grimes, S.; Anderson, D. L.; Bustamante, C. The Bacteriophage Φ29 Portal Motor Can Package DNA against a Large Internal Force. *Nature* **2001**, *413* (6857), 748–752. https://doi.org/10.1038/35099581.

(31) Dame, R. T.; Noom, M. C.; Wuite, G. J. L. Bacterial Chromatin Organization by H-NS Protein Unravelled Using Dual DNA Manipulation. *Nature* **2006**, *444* (7117), 387–390. https://doi.org/10.1038/nature05283.

(32) Dumont, S.; Cheng, W.; Serebrov, V.; Beran, R. K.; Tinoco, I.; Pyle, A. M.; Bustamante, C. RNA Translocation and Unwinding Mechanism of HCV NS3 Helicase and Its Coordination by ATP. *Nature* **2006**, *439* (7072), 105–108. https://doi.org/10.1038/nature04331.

(33) Strick, T. R.; Croquette, V.; Bensimon, D. Single-Molecule Analysis of DNA Uncoiling by a Type II Topoisomerase. *Nature* **2000**, *404* (6780), 901–904. https://doi.org/10.1038/35009144.

(34) Koster, D. A.; Croquette, V.; Dekker, C.; Shuman, S.; Dekker, N. H. Friction and Torque Govern the Relaxation of DNA Supercoils by Eukaryotic Topoisomerase IB. *Nature* **2005**, *434* (7033), 671–674. https://doi.org/10.1038/nature03395.

(35) Leger, J. F.; Robert, J.; Bourdieu, L.; Chatenay, D.; Marko, J. F. RecA Binding to a Single Double-Stranded DNA Molecule: A Possible Role of DNA Conformational Fluctuations. *Proc. Natl. Acad. Sci. U. S. A.* **1998**, *95* (21), 12295–12299. https://doi.org/10.1073/pnas.95.21.12295.

(36) Forget, A. L.; Kowalczykowski, S. C. Single-Molecule Imaging of DNA Pairing by RecA Reveals a Three-Dimensional Homology Search. *Nature* **2012**, *482* (7385), 423–427. https://doi.org/10.1038/nature10782.

(37) Zhang, X. H.; Halvorsen, K.; Zhang, C.-Z. Z.; Wong, W. P.; Springer, T. A. Mechanoenzymatic Cleavage of the Ultralarge Vascular Protein von Willebrand Factor. *Science* **2009**, *324* (5932), 1330–1334. https://doi.org/10.1126/science.1170905.

(38) Halvorsen, K.; Schaak, D.; Wong, W. P. Nanoengineering a Single-Molecule Mechanical Switch Using DNA Self-Assembly. *Nanotechnology* **2011**, *22* (49), 494005. https://doi.org/10.1088/0957-4484/22/49/494005.

(39) Liphardt, J.; Onoa, B.; Smith, S. B.; Tinoco, I.; Bustamante, C. Reversible Unfolding of Single RNA Molecules by Mechanical Force. *Science (80-.).* **2001**, *292* (5517), 733–737. https://doi.org/10.1126/SCIENCE.1058498.

(40) Kim, J.; Zhang, C.-Z.; Zhang, X.; Springer, T. A. A Mechanically Stabilized Receptor-Ligand Flex-Bond Important in the Vasculature. *Nature* **2010**, *466* (7309), 992–995. https://doi.org/10.1038/nature09295.

(41) Kaiser, C. M.; Goldman, D. H.; Chodera, J. D.; Tinoco, I.; Bustamante, C. The Ribosome Modulates Nascent Protein Folding. *Science* **2011**, *334* (6063), 1723–1727. https://doi.org/10.1126/science.1209740.

(42) Seeman, N. C. An Overview of Structural DNA Nanotechnology. *Mol. Biotechnol.* **2007**, *37* (3), 246–257. https://doi.org/10.1007/s12033-007-0059-4.

(43) Pinheiro, A. V.; Han, D.; Shih, W. M.; Yan, H. Challenges and Opportunities for Structural DNA Nanotechnology. *Nat. Nanotechnol.* **2011**, *6* (12), 763–772. https://doi.org/10.1038/nnano.2011.187.

(44) WATSON, J. D.; CRICK, F. H. C. Molecular Structure of Nucleic Acids: A Structure for Deoxyribose Nucleic Acid. *Nature* **1953**, *171* (4356), 737–738. https://doi.org/10.1038/171737a0.

(45) Smith, S. B.; Cui, Y.; Bustamante, C. Overstretching B-DNA: The Elastic Response of Individual Double-Stranded and Single-Stranded DNA Molecules. *Science (80-.).* **1996**, *271* (5250), 795–799. https://doi.org/10.1126/SCIENCE.271.5250.795.

(46) Paik, D. H.; Perkins, T. T. Overstretching DNA at 65 PN Does Not Require Peeling from Free Ends or Nicks. *J. Am. Chem. Soc.* **2011**, *133* (10), 3219–3221. https://doi.org/10.1021/ja108952v.

(47) King, G. A.; Gross, P.; Bockelmann, U.; Modesti, M.; Wuite, G. J. L.; Peterman, E. J. G. Revealing the Competition between Peeled SsDNA, Melting Bubbles, and S-DNA during DNA Overstretching Using Fluorescence Microscopy. *Proc. Natl. Acad. Sci. U. S. A.* **2013**, *110* (10), 3859–3864. https://doi.org/10.1073/pnas.1213676110.

(48) Zhang, X.; Chen, H.; Le, S.; Rouzina, I.; Doyle, P. S.; Yan, J. Revealing the Competition between Peeled SsDNA, Melting Bubbles, and S-DNA during DNA Overstretching by Single-Molecule Calorimetry. *Proc. Natl. Acad. Sci. U. S. A.* **2013**, *110* (10), 3865–3870. https://doi.org/10.1073/pnas.1213740110.

(49) Schakenraad, K.; Biebricher, A. S.; Sebregts, M.; ten Bensel, B.; Peterman, E. J. G.; Wuite, G. J. L.; Heller, I.; Storm, C.; van der Schoot, P. Hyperstretching DNA. *Nat. Commun.* **2017**, *8* (1), 2197. https://doi.org/10.1038/s41467-017-02396-1.

(50) Rao, S. N.; Kollman, P. A. Molecular Mechanical Simulations on Double Intercalation of 9-Amino Acridine into d(CGCGCGC) X d(GCGCGCG): Analysis of the Physical Basis for the Neighbor-Exclusion Principle. *Proc. Natl. Acad. Sci. U. S. A.* **1987**, *84* (16), 5735–5739. https://doi.org/10.1073/pnas.84.16.5735.

(51) Bosaeus, N.; El-Sagheer, A. H.; Brown, T.; Smith, S. B.; Akerman, B.; Bustamante, C.; Nordén, B. Tension Induces a Base-Paired Overstretched DNA Conformation. *Proc. Natl. Acad. Sci. U. S. A.* **2012**, *109* (38), 15179–15184. https://doi.org/10.1073/pnas.1213172109.

(52) Biebricher, A. S.; Heller, I.; Roijmans, R. F. H.; Hoekstra, T. P.; Peterman, E. J. G.; Wuite, G. J. L. The Impact of DNA Intercalators on DNA and DNA-Processing Enzymes Elucidated through Force-Dependent Binding Kinetics. *Nat. Commun.* **2015**, *6*, 7304.

https://doi.org/10.1038/ncomms8304.

(53) Almaqwashi, A. A.; Paramanathan, T.; Rouzina, I.; Williams, M. C. Mechanisms of Small Molecule–DNA Interactions Probed by Single-Molecule Force Spectroscopy. *Nucleic Acids Res.* **2016**, *44* (9), 3971–3988. https://doi.org/10.1093/nar/gkw237.

(54) Murade, C. U.; Subramaniam, V.; Otto, C.; Bennink, M. L. Interaction of Oxazole Yellow Dyes with DNA Studied with Hybrid Optical Tweezers and Fluorescence Microscopy. *Biophys. J.* **2009**, *97* (3), 835–843. https://doi.org/10.1016/j.bpj.2009.05.024.

(55) Kleimann, C.; Sischka, A.; Spiering, A.; Tönsing, K.; Sewald, N.; Diederichsen, U.; Anselmetti, D. Binding Kinetics of Bisintercalator Triostin a with Optical Tweezers Force Mechanics. *Biophys. J.* **2009**, *97* (10), 2780–2784. https://doi.org/10.1016/j.bpj.2009.09.001.

(56) Backer, A. S.; Biebricher, A. S.; King, G. A.; Wuite, G. J. L.; Heller, I.; Peterman, E. J. G. Single-Molecule Polarization Microscopy of DNA Intercalators Sheds Light on the Structure of S-DNA. *Sci. Adv.* **2019**, *5* (3), eaav1083. https://doi.org/10.1126/sciadv.aav1083.

(57) Bustamante, C.; Marko, J. F.; Siggia, E. D.; Smith, S. Entropic Elasticity of Lambda-Phage DNA. *Science* **1994**, *265* (5178), 1599–1600. https://doi.org/10.1126/science.8079175.

(58) Spielmann, H. P.; Wemmer, D. E.; Jacobsen, J. P. Solution Structure of a DNA Complex with the Fluorescent Bis-Intercalator TOTO Determined by NMR Spectroscopy. *Biochemistry* **1995**, *34* (27), 8542–8553. https://doi.org/10.1021/bi00027a004.

(59) Günther, K.; Mertig, M.; Seidel, R. Mechanical and Structural Properties of YOYO-1 Complexed DNA. *Nucleic Acids Res.* **2010**, *38* (19), 6526–6532. https://doi.org/10.1093/nar/gkq434.